PINK1-parkin-mediated mitophagy generates somatic mosaicism of the mitochondrial genome

Arnaud Ahier[1], Nadia Cummins[1], Chuan-Yang Dai[1], Jürgen Götz[1] and Steven Zuryn[1]*.

[1] *Clem Jones Centre for Ageing Dementia Research, Queensland Brain Institute, The University of Queensland, Brisbane, Australia, 4072.*

**Corresponding author.*

Running title: PINK-1-parkin determines mtDNA mosaicism

Keywords: Mitochondria, mtDNA, mitophagy, PINK1, parkin, heteroplasmy, proteotoxicity

Abstract

The composition of the mitochondrial DNA (mtDNA) in each cell is in constant flux through processes of mutation, replication, and degradation. In multiple species, certain tissues consistently harbour greater loads of mtDNA mutations relative to others. However, the mechanisms that drive this stereotyped distribution of mtDNA mutations within individuals are unknown. Using *C. elegans* as a model system, we found that mitochondrial autophagy (mitophagy), mediated through the conserved PTEN-induced putative kinase (PINK1) and the E3 ubiquitin-protein ligase parkin, selectively removes mtDNA mutations from specific tissue types. Moreover, neurons in particular were prone to accumulating mtDNA mutations when mitophagy was perturbed genetically, or through the ectopic expression of proteotoxic species that are associated with neurodegenerative diseases. These results suggest that mitophagy deterministically drives differences in heteroplasmy between tissues, and points at the existence of a causal link between proteotoxicity, mitophagy, and mtDNA mutation levels in neurons.

Introduction

Mitochondria act as central hubs for cellular bioenergetics, macromolecule precursor synthesis, redox balance, Ca^{2+} handling, apoptosis, and immunity [1, 2]. These organelles house their own genome (mtDNA), as well as RNA and protein-synthesizing systems, which together code and coordinate the assembly of core subunits of oxidative phosphorylation (OXPHOS), a process that generates adenosine triphosphate, the primary energy substrate of the cell. Although mtDNA lesions that perturb the assembly of OXPHOS enzymes can cause devastating metabolic disorders [3], mutations are buffered by the polyploidy nature of the mitochondrial genome; tens to hundreds of mitochondria can populate each cell, with each

organelle containing multiple copies of mtDNA. As a result, a mixture of multiple mtDNA variants can co-exist within individual cells [4]. This state is termed heteroplasmy, and the factors that influence its dynamics are critical determinants of the pathogenesis of mitochondrial diseases, and possibly a number of age-related conditions, including neurodegeneration, cardiomyopathy, diabetes, and cancer [5-7].

At any given time, an interplay between stochastic and deterministic processes influences cellular heteroplasmy [5]. Mitotic segregation, genetic drift, and the competing effects of homeostatic [8-12] and retrograde signalling pathways, such as the mitochondrial unfolded protein response [9, 10], may contribute to the divergence of heteroplasmy levels between cells, generating heteroplasmy mosaicism. However, there is evidence that specific organs and tissues are prone to accumulating certain mtDNA mutations, leading to a stereotyped pattern of heteroplasmy mosaicism across individuals [13-17]. For example, the caudate, putamen and substantia nigra regions of the human brain show an age-dependent increase in the heteroplasmy levels of the mtDNA^{4977} deletion (a mutant genome harbouring a 4,977bp deletion), relative to the rest of the brain [15]. Stereotyped heteroplasmy differences between tissues have also been observed in *C. elegans*. Here, mtDNA molecules harbouring a large deletion accumulate at different heteroplasmy levels in distinct somatic and germ lineages over time [16]. However, how these non-random patterns of differences in mtDNA heteroplasmy evolve between tissues is still unknown.

Here, we provide evidence that mitochondrial autophagy (mitophagy) – orchestrated through the PINK1/parkin signalling pathway – selectively removes mutant copies of mtDNA in a subset of somatic tissue-types in *C. elegans*, resulting in the formation of mosaic and

73 stereotyped heteroplasmy differences between tissues of individuals. Whereas mitochondria
74 within the nervous system, epidermis and intestine use PINK1 and parkin to maintain low
75 levels of a mitochondrial genome harbouring a large deletion (*uaDf5,* also called ΔmtDNA),
76 mitochondria in the body wall muscles do not. Instead PINK1 and parkin act unselectively
77 against ΔmtDNA in muscles to control total mitochondrial volume. As a result, removing the
78 PINK1/parkin axis equalises heteroplasmy across all tissue types, abolishing mosaicism
79 between organs. Moreover, we found that neurons were most dependent upon PINK1 and
80 parkin for maintaining low heteroplasmy levels of mtDNA, and that proteotoxic threats
81 associated with neurodegenerative disease and mitophagy inhibition enhanced ΔmtDNA
82 heteroplasmy levels in neurons. Together, these results suggest that PINK1-parkin-mediated
83 mitophagy acts deterministically to drive the formation of a mosaic and stereotyped
84 heteroplasmic landscape in individual organisms, and that genetic or proteotoxic
85 interruptions to this process can increase mtDNA mutation levels in the nervous system.
86
87 **Results**
88 In *C. elegans*, somatic tissues display stereotyped heteroplasmy, whereby body wall muscles,
89 epidermis, neurons, and intestine consistently harbour decreasing heteroplasmy levels of
90 mtDNA mutations relative to each other [16]. To determine how this distinct pattern of
91 heteroplasmy is formed, we assessed whether each tissue responded differently to the same
92 mtDNA mutation, a 3.1 kb deletion (*uaDf5*, also called ΔmtDNA; Figure S1A) [18]. The *uaDf5*
93 deletion exists in heteroplasmy with wild-type copies of the mtDNA at a level of
94 approximately 50-60% across populations of animals (Figure S1B) [9, 18]. This deletion
95 disrupts four genes that encode core subunits of the electron transport chain (Figure S1A). At
96 50-60% heteroplasmy, animals display reductions in basal oxygen consumption as well as

97 total respiratory capacity [9], suggesting that they experience mitochondrial dysfunction. In
98 order to determine how ΔmtDNA altered mitochondrial morphology in each tissue, we
99 introduced the ΔmtDNA genome into animals expressing a fluorescent fusion protein
100 (*Mito::mKate2*) that localizes to mitochondria and is controlled by either a pan-neuronal
101 promoter (*rgef-1p*), an intestinal-specific promoter (*ges-1p*), an epidermis-specific promoter
102 (*dpy-7p*), or a body wall muscle-specific promoter (*myo-3p*). While gross morphology
103 remained unaltered, three-dimensional reconstruction of fluorescence images acquired from
104 each strain revealed that the mitochondrial volume changed in response to the presence of
105 ΔmtDNA in a tissue-dependent manner (Figure 1A-H and Figure S2). The volume of the
106 mitochondrial network was highly increased in the epidermis, only mildly increased in
107 neurons and intestine (Figure 1A-C and 1E-G), and unchanged in body wall muscles (Figure 1D
108 and H). This revealed that when threatened with a common mtDNA defect, distinct tissue
109 types responded uniquely and independently of each other, hinting at the possibility that
110 tissue-specific differences in mitochondrial physiology could generate disparity in ΔmtDNA
111 heteroplasmy.
112
113 Because heteroplasmy is directly determined by the net effect of the propagation and
114 degradation of mutations, we next investigated how mitochondria within each tissue type
115 altered mtDNA copy numbers in response to the presence of ΔmtDNA. To this end, we
116 performed cell-type-specific mitochondrial affinity purification (Figure S3) to separate and
117 isolate intact mitochondria from each tissue type of animals that harboured either wild-type
118 or both mutant and wild-type genomes. Mitochondria from each of the four tissues were
119 purified from transgenic strains carrying *TOMM-20::mKate2::HA* in which the outer surface
120 of the mitochondria was labelled with a hemagglutinin (HA) epitope in a tissue-specific

121 manner. Using anti-HA antibody-coated beads, mitochondria from each tissue type were
122 affinity-purified from homogenates and the number of individual mitochondria within each
123 sample was quantified before their DNA extracted to determine the copy number of genomes
124 per organelle using a fluorescent probe-based qPCR assay. We found that as a result of the
125 presence of ΔmtDNA the mtDNA copy number per mitochondrion increased in all tissues
126 except epidermis, with the largest absolute increase in copy number per organelle observed
127 in mitochondria isolated from body wall muscles (Figure 2A-D). This suggests that muscle
128 cells increase mtDNA replication in the presence of ΔmtDNA more than any other somatic
129 tissue investigated here. Because the ΔmtDNA genome is smaller in size than its wild-type
130 counterpart, it has an inherent replicative advantage [17, 19]. As such, any enhanced rates of
131 mtDNA replication in muscle cells may disproportionately increase heteroplasmy over time
132 and contribute to greater heteroplasmy loads.
133
134 The heightened mtDNA copy numbers in body wall muscles may reflect the comparatively
135 demanding energetic function that this tissue performs. Body wall muscles include four
136 quadrants of somatic muscle bundles, each of which consists of 23-24 cells arranged into
137 staggered pairs that stretch longitudinally from the head to the tail of the animal [20]. The
138 coordinated contractile activities of these bundles produce powerful sinusoidal body bends
139 that drive locomotion. Increasing the total mtDNA copy number in body wall muscles may
140 help to functionally compensate for ΔmtDNA, in a similar fashion as recently shown in mouse
141 sperm harbouring high levels of mtDNA mutations [21]. Indeed, under strenuous conditions
142 (performing the thrashing assay, see Materials and Methods), muscle function was
143 unperturbed in the presence of ΔmtDNA, even when we forced heteroplasmy to very high
144 loads (93.39 ± 0.34%) by genetically bottlenecking and selecting individual animals with high

145 ΔmtDNA levels across several generations (Figure 2E-H and Figure S4). Furthermore, body
146 wall muscle function was still unperturbed in animals with high ΔmtDNA heteroplasmy at
147 older ages (Figure 2G and H and Figure S4). Therefore, increasing mtDNA copy number may
148 functionally compensate for ΔmtDNA, particularly in energetically demanding cells such as
149 muscle, but it could also act to promote the propagation of mutant genomes with a replicative
150 advantage leading to the development of tissue disparity in heteroplasmy over time.
151
152 In addition to DNA replication, ΔmtDNA heteroplasmy can be modified through selective
153 degradation processes. Mitophagy contributes to mitochondrial turnover by selectively
154 destroying depolarized mitochondria harbouring mtDNA mutations [9, 10, 18], and it can be
155 triggered by a diverse array of cellular events, including cellular differentiation, and in
156 response to physiological cues, such as cellular activity and nutrient levels [22]. As such,
157 mitophagy may operate under distinct parameters in different cell types, which, in the
158 presence of ΔmtDNA mutations, could contribute to determining the heteroplasmy levels of
159 specific tissues and organs.
160
161 To test this idea, we introduced the ΔmtDNA mutation into double-mutant strains with null
162 deletions in the genes *pink-1* (PINK1) and *pdr-1* (parkin)[23], key mediators of mitophagy in
163 multiple species including *C. elegans* [24-27]. PINK1 normally induces mitophagy by
164 accumulating on the outer mitochondrial membrane of defective organelles, where it recruits
165 the E3 ubiquitin ligase parkin [28]. Parkin decorates the surface of these mitochondria with
166 polyubiquitin chains, thereby inducing engulfment by autophagosomes and destruction
167 following fusion with lysosomes [29]. The *pink-1(tm1779);pdr-1(gk448)* mitophagy-deficient
168 mutant animals harbouring ΔmtDNA were crossed to transgenic animals carrying the *TOMM-*

169 *20::mKate2::HA* transgene expressed under the individual tissue-specific promoters (muscle,
170 intestine, epidermis and neurons), and intact mitochondria were isolated from each tissue
171 using affinity purification (Figure 3A) [16]. To eliminate the possibility of any population
172 variability affecting our analyses, we compared mitochondria purified from each tissue to the
173 total mitochondria (homogenate) from the same samples. In addition, we performed the
174 same experiments in animals in which mitochondria from all cell types were purified using a
175 strain expressing *TOMM-20::mKate2::HA* under the ubiquitous promoter *eft-3p*. As expected,
176 ΔmtDNA heteroplasmy levels were not different between total mitochondria (homogenate)
177 and mitochondria affinity purified from all cell types (ubiquitous) in both wild-type and *pink-*
178 *1*;*pdr-1*backgrounds (Figure 3B), confirming that deficiencies in PINK-1 and PDR-1 did not
179 influence the mitochondrial isolation procedure. Deleting *pink-1* and *pdr-1*, however, resulted
180 in a significant increase in ΔmtDNA heteroplasmy levels in mitochondria purified from
181 neurons, intestine, and epidermis (Figure 3C-E), suggesting that PINK-1 and PDR-1 operate
182 within these tissues to reduce ΔmtDNA heteroplasmy. Neither *pink-1* nor *pdr-1* appeared to
183 affect mtDNA replication, as mtDNA copy number was unchanged in *pink-1*;*pdr-1* double
184 mutant backgrounds (Figure 3H). Instead, and as previously demonstrated [8-10], one
185 plausible explanation for our finding is that mitophagy preferentially targets and destroys
186 mitochondria that harbour the highest loads of ΔmtDNA. Interestingly, this activity was not
187 conserved in the body wall muscles. Removal of *pink-1* and *pdr-1* had no effect on ΔmtDNA
188 heteroplasmy levels in this tissue (Figure 3F), suggesting that mitophagy has distinct roles,
189 including in mtDNA quality control, in the different tissue types. The lack of mitophagy-driven
190 selectivity against ΔmtDNA in muscle cells may lead to the formation of heteroplasmy
191 disparity between this tissue and other somatic tissues. In support of this notion, differences

192 in ΔmtDNA heteroplasmy between muscle and other tissues was abolished when *pink-1* and
193 *pdr-1* were deleted (Figure 3G, G', and G'').
194
195 It is possible that PINK-1-PDR-1-mediated mitophagy is inactive in body wall muscle cells, and
196 that deleting the *pink-1* and *pdr*-1 would therefore be inconsequential to ΔmtDNA
197 heteroplasmy in this tissue. However, we found that a PINK-1::GFP reporter driven by its
198 native promoter [30] was expressed in the muscle cells, in addition to the other cell types
199 studied here (Figure 4A-D). A translational GFP::PDR-1 reporter is also expressed in body wall
200 muscles in *C. elegans*, suggesting that PDR-1 is normally present in this tissue [23]. Moreover,
201 removal of *pink-1* and *pdr-1* dramatically increased mitochondrial volume in the muscle cells,
202 suggesting that mitophagy is used to constrain the mitochondrial network size in this cell type
203 (Figure S5). Indeed, previous studies have found that RNA inactivation (RNAi) of *pink-1* also
204 increased mitochondrial volume in the body wall muscle cells of *C. elegans* [25]. This is in
205 contrast to neurons, intestine, and epidermis, in which *pink-1* and *pdr-1* removal had no effect
206 on mitochondrial volume (Figure S5). Taken together, these results suggest that PINK-1-PDR-
207 1-mediated mitophagy performs different roles in each tissue type, which leads to the
208 development of distinct and stereotyped heteroplasmy levels in different organs.
209
210 Our results indicate that the activity of PINK-1-PDR-1-mediated mitophagy can determine
211 ΔmtDNA heteroplasmy in neurons, intestinal cells, and epidermal cells. We recently
212 demonstrated that proteotoxic tau, a protein that forms aggregates in tauopathies such as
213 Alzheimer's disease [31], perturbs parkin translocation to the mitochondria, and that human
214 tau expressed in the *C. elegans* nervous system inhibits mitophagy [24]. Because inactivating
215 *pink-1* and *pdr-1* increased ΔmtDNA heteroplasmy levels in neurons more than in any other

216 investigated tissue type, we next determined whether the expression of tau could also
217 increase heteroplasmy levels in the nervous system. We constructed strains harbouring
218 ΔmtDNA and expressing human tau (hTau) in the nervous system (*aex-3p::hTau*) [24] as well
219 as the neuron-specific TOMM-20::mKate2::HA tag. We then performed affinity purification of
220 neuronal mitochondria in these strains and found that hTau significantly increased
221 heteroplasmy (Fig. 4E), suggesting that the expression of mitophagy-inhibiting proteins can
222 increase ΔmtDNA levels in neurons. Other proteotoxic species have also recently been found
223 to inhibit mitophagy in neurons. The expanded polyglutamine (polyQ) tract in mutant forms
224 of the Huntingtin protein (Htt) that cause Huntington disease were recently reported to
225 impede mitophagy in differentiated striatal neurons [32]. Indeed, we found that the
226 expression of a polyglutamine (polyQ) tract (*rgef-1p::Q40::yfp*) [33] in the *C. elegans* nervous
227 recapitulated the effect of hTau and increased ΔmtDNA heteroplasmy in neurons (Fig. 4E).
228 These results suggest that diverse proteotoxic threats associated with a broad range of
229 neurodegenerative diseases may promote the accumulation of mtDNA deletions in the
230 nervous system.
231
232 **Discussion**
233 Polyploidy of the mitochondrial genome gives rise to intercellular and intertissue differences
234 in heteroplasmy, whereby adjacent cells or tissues within the same individual develop
235 different mtDNA mutation loads. Our results suggest that the tissue-specific activities of *pink-*
236 *1* and *pdr-1*, conserved genes that mediate key steps of mitophagy in *C. elegans* [24-27], give
237 rise to stereotyped differences in heteroplasmy between major somatic tissues (Fig 4F).
238 Furthermore, we have demonstrated that proteotoxic threats that can perturb mitophagy in
239 neurons can increase heteroplasmy levels in the nervous system. Taken together, our results

240 suggest that individual cellular contexts, genetic perturbations, and disease-related
241 proteostatic stresses that can each modify the activity of mitophagy processes, lead to
242 changes in the distribution and abundance of mtDNA mutations throughout an organism.
243
244 Previously, others have shown that mtDNA mutations can alter mitochondrial morphology
245 and mtDNA copy number [18, 34]. Here we have assessed these changes with cell-type-
246 specific resolution and have found that the ΔmtDNA mutation invoked distinct alterations in
247 mitochondrial volume and mtDNA copy number in individual tissues. The fact that each tissue
248 type displays a unique response to an identical mtDNA perturbation suggests that specific
249 changes in mitochondrial physiology are activated under distinct cellular contexts. For
250 example, in the presence of ΔmtDNA, mitochondrial volume in the epidermis increased
251 significantly, but did not change in the body wall muscles. Oppositely, mtDNA copy number
252 per mitochondrion was unchanged in the epidermis, but increased the greatest in muscle
253 cells. These distinct responses may be derived from tissue function and hence energetic
254 requirements. Relative to the epidermal tissue, the energetically strenuous function of the
255 body wall muscle during locomotion may require compensatory increases in mtDNA
256 biogenesis to overcome deficiencies caused by the ΔmtDNA mutation. Indeed, others have
257 found the same to be true in energetically demanding cells. In mice harbouring high levels of
258 mtDNA mutations [35, 36], an increase in total mtDNA copy number in spermatocytes
259 rescued the fertility phenotype and normalized spermatocyte proteome changes, in spite of
260 unaltered mtDNA mutation load [21]. Moreover, increasing mtDNA copy number in mice
261 harbouring a heteroplasmic mtDNA mutation (m.5024C>T) ameliorated pathology in a
262 number of energetically demanding tissues, such as the heart [37]. Even when heteroplasmy
263 was forced to very high values through genetic bottlenecking, we found that muscle function

264 was unperturbed in ΔmtDNA animals, despite the mutational load being the greatest in the
265 body wall muscle cells. Therefore, certain cell types with energetically demanding functions,
266 such as muscle, may preferentially compensate for the effect of deleterious mtDNA mutations
267 by increasing total mtDNA copy number, rather than by clearing the mtDNA mutation through
268 processes such as mitophagy. An unintended consequence of such a strategy may be to
269 propagate those mtDNA mutations that have a replicative advantage, such as large deletions.
270
271 Although enhanced mtDNA propagation may help to contribute to heightened ΔmtDNA
272 heteroplasmy levels in body wall muscles, our results indicate that the removal of *pink-1* and
273 *pdr-1* was sufficient to equalise ΔmtDNA heteroplasmy levels across all tissue types. This
274 suggests that the tissue-specific activities of PINK-1-PDR-1-mediated mitophagy alone can
275 drive the formation of heteroplasmy disparity between tissues. While in neurons, intestinal
276 cells, and epidermal cells, deleting *pink-1* and *pdr-1* resulted in an increase in ΔmtDNA
277 heteroplasmy, levels remained unchanged in muscle cells. This suggests that whereas PINK-
278 1-PDR-1-mediated mitophagy selects against the ΔmtDNA mutation in neurons, intestine, and
279 epidermis, it does not do so in body wall muscle. Instead, mitophagy acts to constrain the
280 volume of the mitochondrial network in the body wall muscles, rather than selectively
281 reducing the heteroplasmy levels of ΔmtDNA mutations. This indicates that PINK-1-PDR-1-
282 mediated mitophagy performs distinct roles in different cell types, which predisposes certain
283 tissues and organs to the accumulation of ΔmtDNA.
284
285 In humans, large mtDNA deletions have been shown to accumulate in specific regions of the
286 brain during ageing [15]. Although there is strong evidence that PINK1-parkin-mediated
287 mitophagy occurs in mammalian neurons [38, 39], it is not known whether differences in the

288 activity of mitophagy plays a role in specifying the heteroplasmy levels of mtDNA deletions
289 within distinct regions of the brain. In mice homozygous for a proofreading deficiency in DNA
290 polymerase γ, which induces a high level of mtDNA single nucleotide mutations [35, 36],
291 parkin knockout significantly increases the levels of pathogenic mtDNA mutations in the
292 striatum [40]. Moreover, mutations in Pink1 [41] and parkin [42] can lead to early onset
293 Parkinson's disease, and substantia nigra neurons in Parkinson's disease patients have high
294 levels of mtDNA deletions [43, 44]. Although we did not examine subsets of neurons in this
295 study, our results suggest that neurons in general are the most vulnerable to increases in
296 heteroplasmy when mitophagy is perturbed. Therefore, our work demonstrates that
297 mutations in Pink1 and parkin have a widely conserved effect across phyla of enhancing the
298 accumulation of mtDNA deletions in neurons, which may perturb their function and cause
299 disease.
300
301 In addition to Pink1 and parkin mutations, we found that toxic proteins associated with
302 neurodegenerative diseases other than Parkinson's disease also increase heteroplasmy.
303 Overexpression in neurons of hTau, as well as a polyQ tract, significantly increased ΔmtDNA
304 heteroplasmy levels in the *C. elegans* nervous system. To our knowledge, this represents the
305 first reported incidence of proteotoxicity increasing the cellular load of mtDNA mutations.
306 Interestingly, similar proteotoxic species have been recently reported to inhibit mitophagy in
307 neurons. Via its projection domain, hTau can associate with Parkin in the cytoplasm and
308 specifically impair its translocation to the surface of defective mitochondria in human
309 neuroblastoma cells [24]. In addition, a polyQ tract within expanded mutant versions of the
310 Huntingting protein can prevent the formation of the Beclin1-Vps34 initiation complex,
311 negatively affecting the efficiency of mitophagy in post-mitotic striatal neurons [32]. These

312 results demonstrate that perturbing mitophagy indirectly with proteotoxicity has the same
313 effect as perturbing mitophagy genetically through mutations in *pink-1* and *pdr-1*. They also
314 demonstrate that toxic proteins associated with diverse neurodegenerative diseases can
315 modify the genetic landscape of the mitochondrial genome in neurons and provide evidence
316 that two of the most common hallmarks of neurodegeneration - proteotoxicity and
317 mitochondrial dysfunction - may converge at the level of the mitochondrial genome.
318

319 **Materials and Methods**

320 ***C. elegans* strains and culture**. LB138 *him-8(e1489) IV; uaDf5/+*; EG8078 *oxTi185 I; unc-*
321 *119(ed3) III;* BR4006 *pink-1(tm1779) II; byEx655 [pink-1p::pink-1::GFP; myo-2p::mCherry;*
322 *herring sperm DNA]*; VC1024 *pdr-1(gk448) III*; AM101 *rmIs110 [rgef-1p::Q40::YFP]* and wild-
323 type (N2) were acquired from the *Caenorhabditis* Genetics Center (CGC), University of
324 Minnesota, USA, which is funded by the NIH Office of Research Infrastructure Programs (P40
325 OD010440). APD178 *apdIs11 [aex-3p::tau4RIN + coel::gfp]* were kindly provided by Dr H.
326 Nicholas (The University of Sydney, Sydney, Australia). *C. elegans* culture and maintenance
327 were performed according to standard protocols [45]. The transgenic strains used for cell-
328 specific mitochondrial purification experiments were generated as previously described [16].
329

330 **Cell-specific mitochondrial affinity purification (CS-MAP).** CS-MAP was performed as
331 previously described [16]. Heteroplasmy in mitochondria derived from different cell types
332 was investigated across very large populations of pooled animals (>10,000 individuals). This
333 approach enabled population-scale trends to be resolved by overcoming confounding
334 influences that can be introduced by the presence of stochastic inter-individual variations.
335 Briefly, 10,000 to 20,000 L4 staged worms were grown on 2 x 150 mm NGM plates seeded

336 with *E. coli* OP50 bacteria. Worms were homogenized into a hypotonic buffer [50 mM KCl,
337 110 mM mannitol, 70 mM sucrose, 0.1 mM EDTA (pH 8.0), 5 mM Tris-HCl (pH 7.4)] with a
338 dounce homogenizer and the subsequent crude mitochondrial fraction was enriched by
339 differential centrifugations. The mitochondria were then isolated from this fraction using anti-
340 HA (influenza hemagglutinin) magnetic beads (Pierce). The beads were washed and
341 resuspended in 20 µl of hypotonic buffer. All CS-MAP experiments were repeated in at least
342 three independent experiments and data for each genetic background were obtained at
343 similar times to those previously reported for control wild-type backgrounds [16].
344
345 **mtDNA extraction and quantitative PCR of heteroplasmy**. For all mtDNA analyses, total input
346 and affinity-purified mitochondria were lysed and extracted using phenol-chloroform-isoamyl
347 alcohol, followed by an ethanol precipitation. Extracted DNA was resuspended in 10 mM Tris-
348 HCl (pH 8), 0.1 mM EDTA. Multiplex quantitative PCR was then performed using the Luna
349 Universal Probe qPCR Master Mix (ref M3004, NEB), a Roche LightCycler or Rotor Gene Q real-
350 time PCR (Qiagen) machine and Rotor Gene Q pure detection software (V2.3.1). The primers
351 5'-cgtaagaaaatcaaaatatggtataattgg-3', 5'-aaaatgttacgatccttattaataaagc-3', 5'-
352 gcagagatgtttattgaagctgac-3' and the probes 5'-HEX/tgaggccag/ZEN/ttcatattgttccaga
353 gtg/IABKFQ-3' (Iowa Black FQ) and 5'-6-FAM/ccatccgtg/ZEN/ctagaagacaaagaatttc/IABKFQ-3'
354 were used to quantify the wild-type mtDNA and ΔmtDNA levels. Calculations of mtDNA copies
355 per mitochondrion were derived from the quantification of purified organelles in individual
356 samples, as previously performed [16]. Control wild-type values have been previously
357 reported by Ahier et al., 2018 [16].
358
359 **Quantification of mtDNA copy number**

360 Ten (10) L4 worms from each genetic background were lysed in 10 µl of standard lysis buffer
361 supplemented with 200 ng ml−1 proteinase K and incubated at 65°C for 2 h, followed by heat-
362 inactivation at 95 °C for 15 min. A 1/50 dilution of the lysate was used for subsequent
363 quantitative PCR. The Sensifast SYBR no-rox Kit (ref. BIO-98005, Bioline) and a Rotor Gene Q
364 Real-Time PCR (Qiagen) Machine, with Rotor Gene Q pure detection software (V2.3.1), were
365 used for quantitative PCR (qPCR). The primers SZ35 (5'-AGGCTAAGCCGGGGTAAGTT-3') and
366 SZ36 (5'-GCCAAAAGCTTAAACTGCGG-3') were used to quantify the nuclear DNA and the
367 primers AA178 (5'-CATACCGAATAAACATCAGGGTAATCT-3'), AA179 (5'-
368 ACGGGTGTTACACTATGATGAAGA-3') were used to quantify the mtDNA levels. The cycle
369 conditions were 95°C for 10 min, followed by 45 cycles of 95°C for 15 s and 58°C for 40 s.
370 Primer efficiencies were determined by amplifying a series of exponential dilutions (1 to
371 10^{-8} ng) of cloned wild-type mtDNA (pSZ116) and *ges-1* promoter (pSZ57) fragments,
372 confirming an equivalent efficiency of both sets of primers (91.2% for SZ35 and SZ36 and
373 90.6% for AA178 and AA179).
374
375 **Image acquisition and processing**. Imaging was performed on live animals mounted on a 2%
376 agarose pad on glass slides with 1 mM levamisole (Sigma). For quantification of purified
377 mitochondria, we visualized fluorescence using a Zeiss Z2 imager microscope with a Zeiss
378 Axiocam 506 mono camera and Zen2 (version 2.0.0.0) software. Mitochondria were counted
379 with the aid of the Image J Grid plugin, and comparisons were made on the same
380 immunoprecipitation volume for each sample. For 3D reconstruction, imaging/analysis was
381 performed at the Queensland Brain Institute's Advanced Microscopy Facility using a spinning-
382 disk confocal system (Marianas; 3I, Inc.) consisting of an Aanio Observer Z1 (Carl Zeiss)
383 equipped with a CSU-W1 spinning-disk head (Yokogawa Corporation of America), ORCA-

384 Flash4.0 v2 sCMOS camera (Hamamatsu Photonics), and 20x 0.8 NA PlanApo and 40x 1.2 NA
385 C-Apo objectives. Image acquisition was performed using SlideBook 6.0 (3I, Inc). 3D
386 reconstruction and mitochondrial volume calculations were performed using 3D rendering in
387 Imaris software (version 8.4.1, Bitplane).
388
389 **Thrashing assays**. Thrashing assays were performed on worms suspended in 40 µl of M9
390 buffer on a hydrophobic slide (ref G350308BK, ProSciTech). After an initial 3 min period, a 30
391 second video sequence of the thrashing animals was recorded using a Nikon SMZ745T
392 stereomicroscope and a TrueChrome IIS camera (Tucsen Photonics). The number of body
393 bends per minute, as well as other mobility metrics, was determined using CeleST Computer
394 Vision Software as described previously [46].
395
396 **Statistics and reproducibility**. The statistical analyses are described for each figure. Generally,
397 an unpaired parametric two-tailed *t*-test was used to determine the significance of
398 comparisons made between two data sets, unless otherwise noted in the figure legend. One-
399 way analysis of variance (ANOVA) was performed for comparisons across multiple
400 independent samples, using Tukey's multiple comparisons correction. All experiments were
401 reproduced at least 3 times with similar results. All data and biological reagents that support
402 the conclusions of this manuscript are available from the corresponding author on request.
403
404 **Acknowledgements**
405 We are grateful to M. Hilliard and R. Tweedale for comments on the manuscript and members
406 of the Zuryn laboratory for discussions and comments. We also thank A. Gaudin for support
407 with microscopy. Some strains were provided by the CGC, which is funded by the NIH Office

of Research Infrastructure Programs (P40 OD010440). This work was supported by NHMRC Project Grants GNT1128381 and GNT1162553, a Stafford Fox Senior Research Fellowship to S.Z., ARC Discovery grant DP160103812 to J.G. and a University of Queensland International Scholarship to C.Y.D.

Author contributions

A.A. carried out most experiments. N.C., C.Y.D., S.Z. contributed some experiments. J.G. supervised N.C. and contributed to the interpretation of experiments. A.A., N.C., C.Y.D and S.Z. designed and interpreted experiments. A.A. and S.Z. wrote the paper. All authors approved the final manuscript.

Conflict of interest

The authors declare that they do not have any financial or non-financial competing interests.

Figures

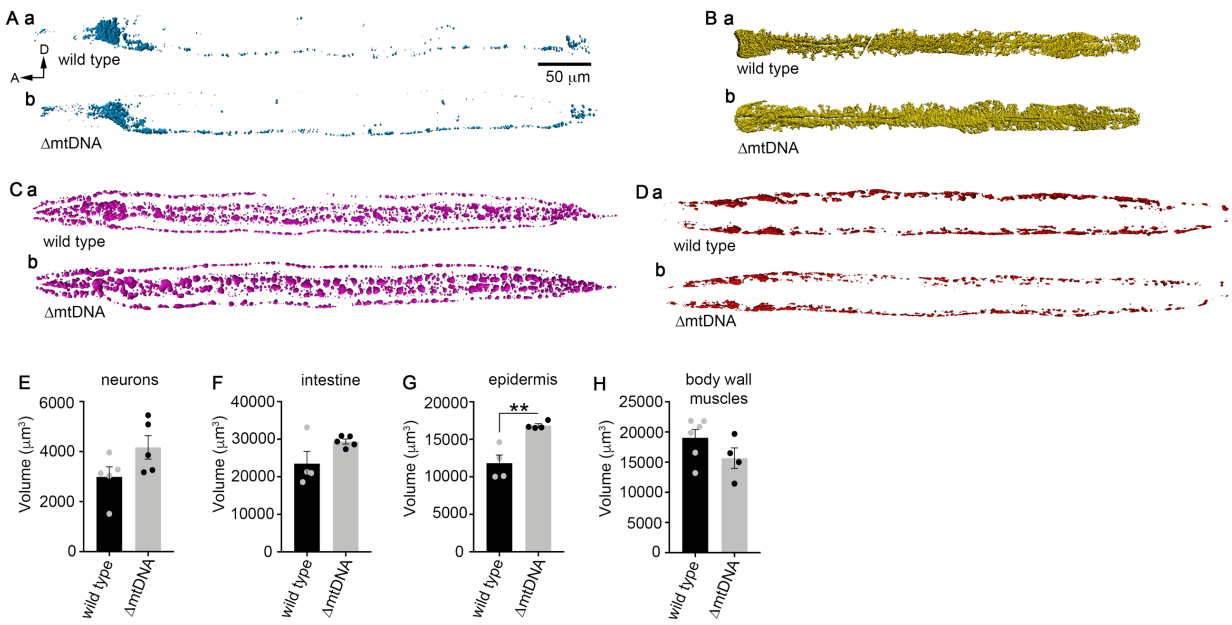

Figure 1. The presence of ΔmtDNA alters mitochondrial volume in a tissue-dependent manner. (**A-D**) Representative three-dimensional reconstructions of *C. elegans'* (**A**) complete nervous system mitochondria, (**B**) intestinal mitochondria, (**C**) epidermal mitochondria, and (**D**) body wall muscle mitochondria in (**a**) wild-type animals and (**b**) animals harbouring ΔmtDNA. Scale bar, 50 μm. (**E-H**) Quantification of mitochondrial volumes from each tissue type. Columns are means ± s.e.m. of individual animals (n = 5). ** = p< 0.01. P values were determined using one-way ANOVA and Tukey's correction.

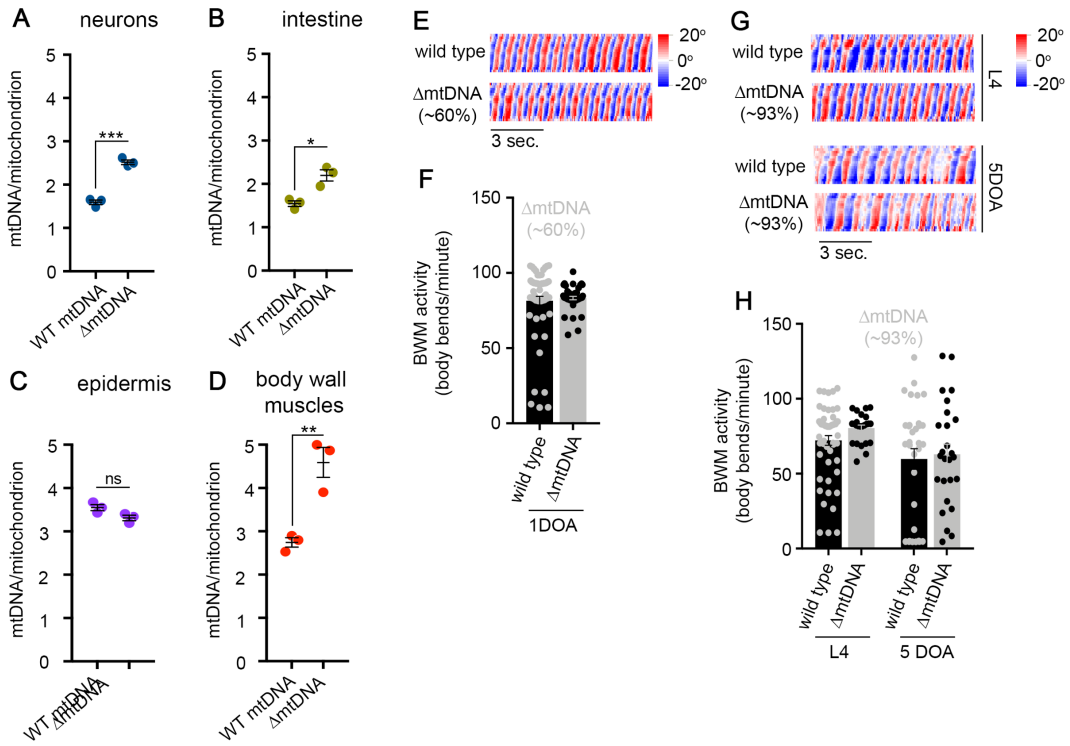

Figure 2. The presence of ΔmtDNA alters mtDNA copy number in a tissue-specific manner. (**A-D**) Quantification of mtDNA molecules per mitochondrion. Each dot represents the average number of mtDNA molecules per mitochondrion from at least 1,000 mitochondria analysed from (**A**) neurons, (**B**) intestinal cells, (**C**) epidermal cells, and (**D**) body wall muscle cells. Bars are means of three biologically independent experiments ± s.e.m. * = $p < 0.05$; ** = $p < 0.01$; *** = $p < 0.001$. *P* values were determined using one-way ANOVA and Tukey's correction. (**E-H**) Animals harbouring wild-type mtDNA or ΔmtDNA have equivalent levels of body wall muscle activity as determined by the thrashing assay. (**E** and **G**) Representative heatmaps of an individual animal's body angle over time as it thrashes in liquid. (**F** and **H**) Quantification of body bends per minute. BWM, body wall muscle. Columns are means ± s.e.m. of individual animals (dots). Two-sided *t*-test. L4, larval stage 4; 1 DOA, 1-day-old adult; 5 DOA, 5-day-old adult.

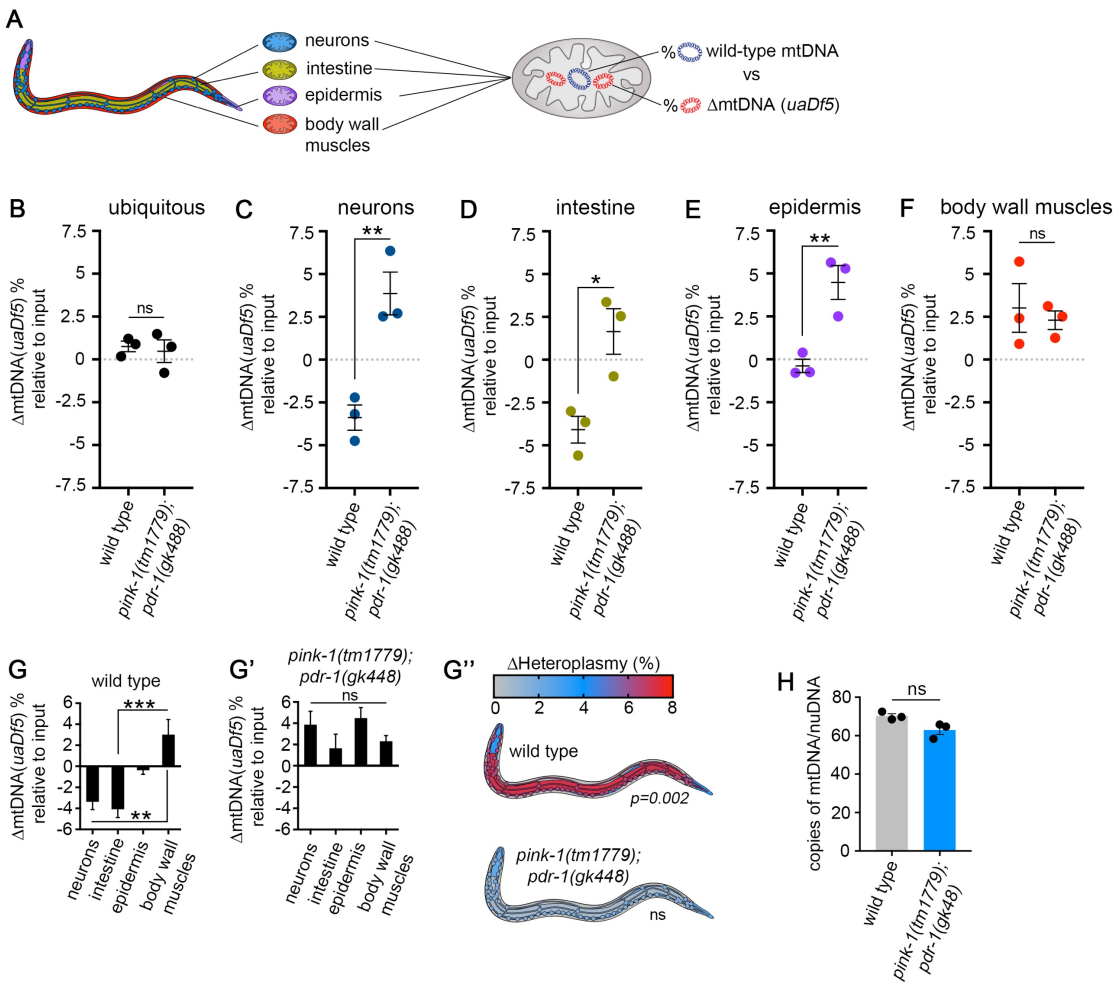

450

451 **Figure 3. Deletion of *pink-1* and *pdr-1* increases heteroplasmy in a tissue-specific manner**

452 **and removes ΔmtDNA mosaicism.** (**A**) Schematic of *C. elegans* and mitochondria originating

453 from major somatic tissue types in which ΔmtDNA (*uaDf5*) heteroplasmy was determined. (**B-**

454 **F**) Percentage of ΔmtDNA in mitochondria purified from each tissue type in L4 animals,

455 relative to total homogenate. Bars are means ± s.e.m. of three independent biological

456 replicates (dots) consisting of ~10,000 animals each. * = $p < 0.05$; ** = $p < 0.01$. *P* values were

457 determined using one-way ANOVA and Tukey's correction. Comparison of heteroplasmy

458 between tissues in (**G**) wild-type animals and (**G'**) *pink-1;pdr-1* double mutants indicates that

459 inter-tissue differences in ΔmtDNA heteroplasmy is lost upon deletion of *pink1* and *pdr-1*.

460 (**G''**) Graphical representation of the loss of stereotyped inter-tissue variation in ΔmtDNA

461 heteroplasmy in *pink-1;pdr-1* double mutant animals. Each tissue type is coloured according
462 to ΔHeteroplasmy, which is the difference in *uaDf5* heteroplasmy relative to BWM. The
463 significance of heteroplasmy variation between tissues was calculated using one-way ANOVA.
464 ** = $p < 0.01$; *** = $p < 0.001$. *P* values were determined using one-way ANOVA and Tukey's
465 correction. (**H**) Quantitative PCR analysis of mtDNA copy number in L4 wild type and *pink-*
466 *1;pdr-1* double mutants. Columns are means ± s.e.m. of three independent biological
467 replicates (dots), each consisting of 10 animals, analysed with a two-sided *t*-test.

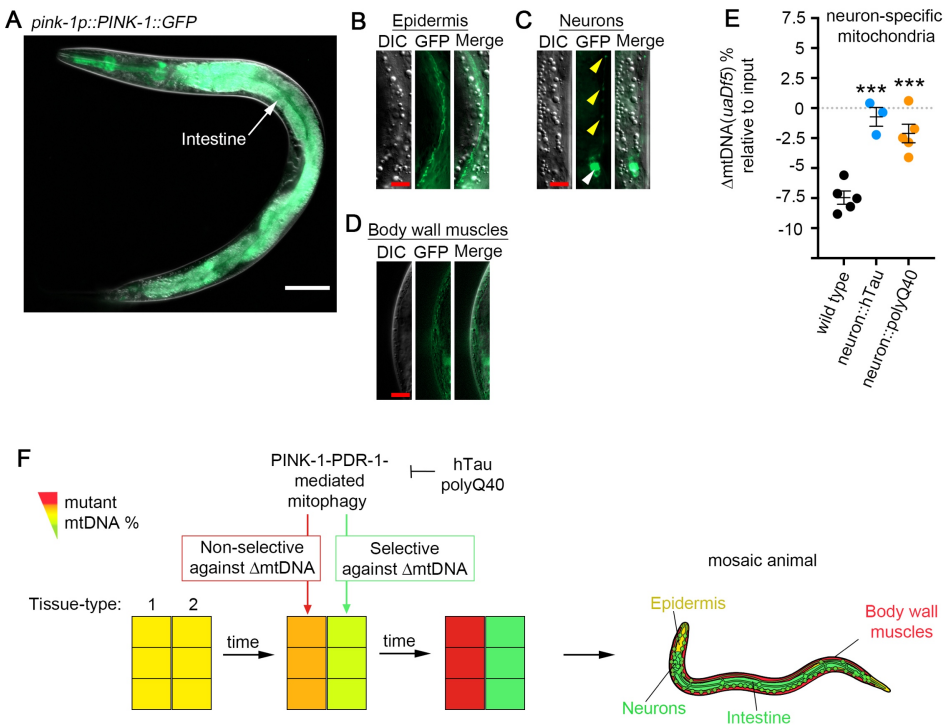

Figure 4. Expression of proteotoxic proteins in neurons increases ΔmtDNA heteroplasmy. (**A**) A *pink-1* translation fluorescent reporter is expressed in most somatic tissues in *C. elegans*, including in the (**A**) intestine, (**B**), epidermis, (**C**) neurons, and (**D**) body wall muscle. Yellow arrowheads indicate the axon, while the white arrowhead indicates the cell body of a neuron. White scale bar, 50μm; red scale bar, 5μm. (**E**) Expression of either human tau (hTau) or a polyglutamine tract (Q40) in neurons increases the heteroplasmy levels of ΔmtDNA (*uaDf5*) in the nervous system. Bars are means ± s.e.m. of at least three independent biological replicates (dots) consisting of ~10,000 animals each performed at day 1 of adulthood. *** = $p < 0.001$. *P* values were determined using one-way ANOVA and Tukey's correction. (**F**) Proposed model that leads to mosaicism of mtDNA. PINK-1-PDR-1-mediated mitophagy displays distinct activities in different tissue types which leads to the formation of a stereotyped pattern of ΔmtDNA heteroplasmy. In neurons, the expression of proteotoxic proteins can inhibit mitophagy, leading to an increase in heteroplasmy in the nervous system.

482 **Supplemental Figure Legends**

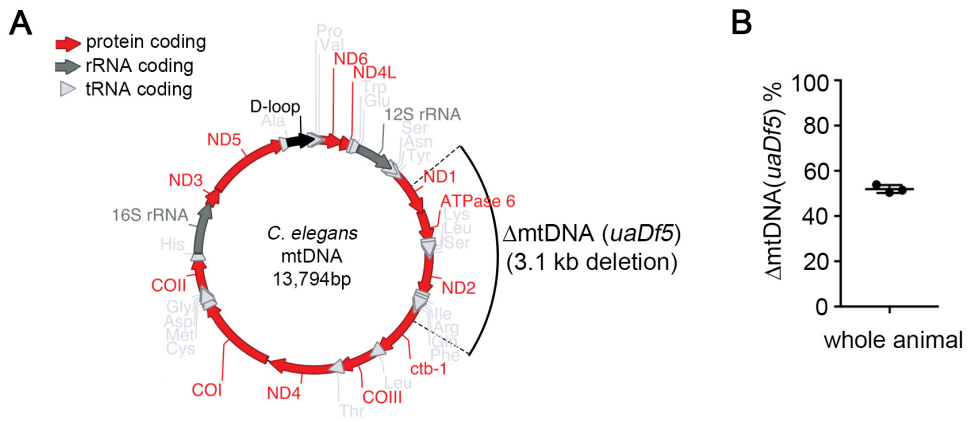

483

484 **Figure S1.**

485 (**A**) Map of *C. elegans* mtDNA showing the location of the 3.1kb *uadF5* deletion. (**B**)

486 Quantification of *uaDf5* heteroplasmy in whole animal extracts. Heteroplasmy was stable at

487 around 50-60% for each of the strains used. Bar represents the mean value of three

488 independent experiments ± s.e.m.

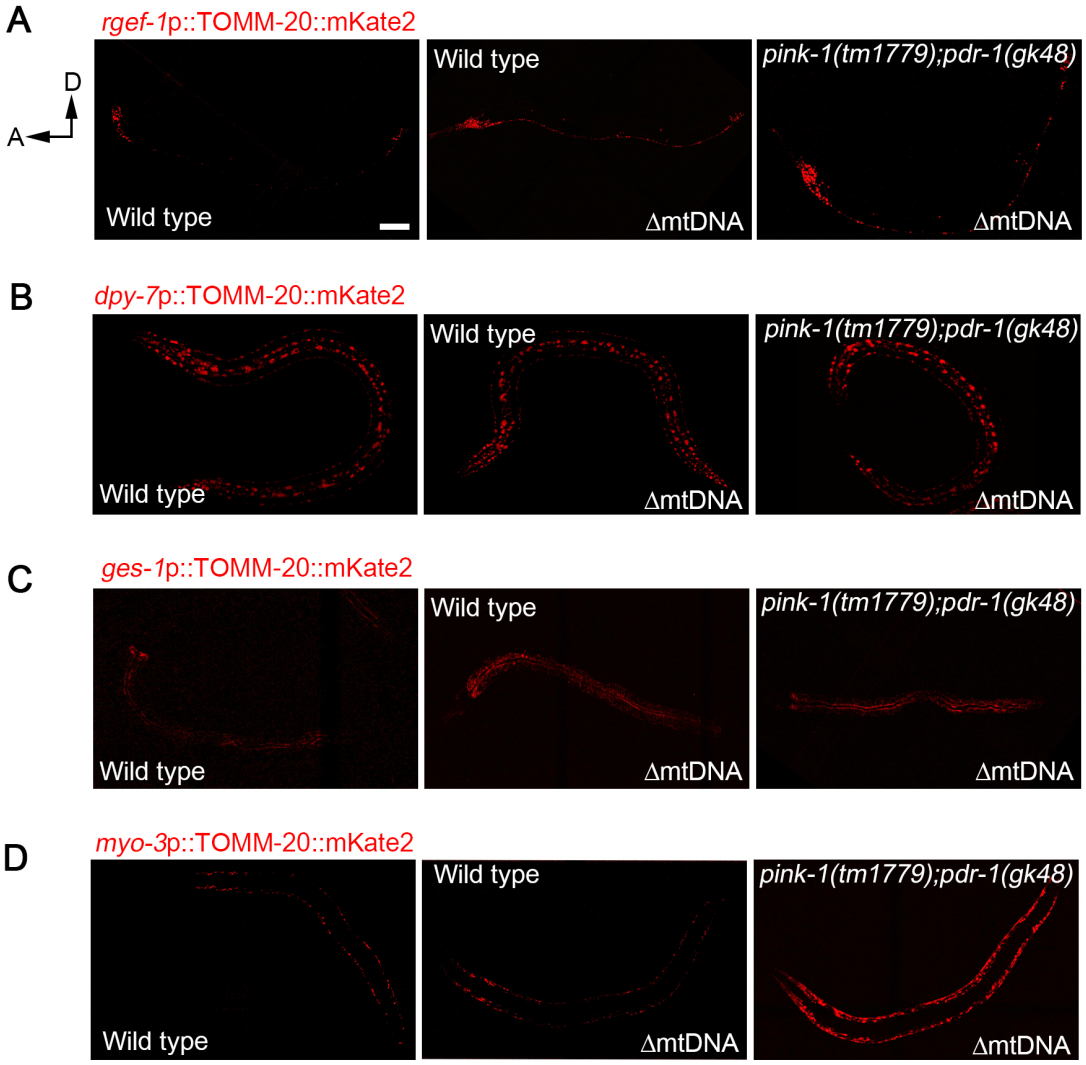

Figure S2. Changes in mitochondrial volume in response to ΔmtDNA and *pink-1/pdr-1* mutation in different cell types. (**A-D**) Representative microimages corresponding to the three-dimensional reconstructions shown in Figure 2. (**A**) complete nervous system mitochondria, (**B**) intestinal mitochondria, (**C**) epidermal mitochondria, and (**D**) body wall muscle mitochondria. Images presented in Figure 2 were reconstructed using Imaris software and straightened using ImageJ for presentation. Scale bar, 50μm.

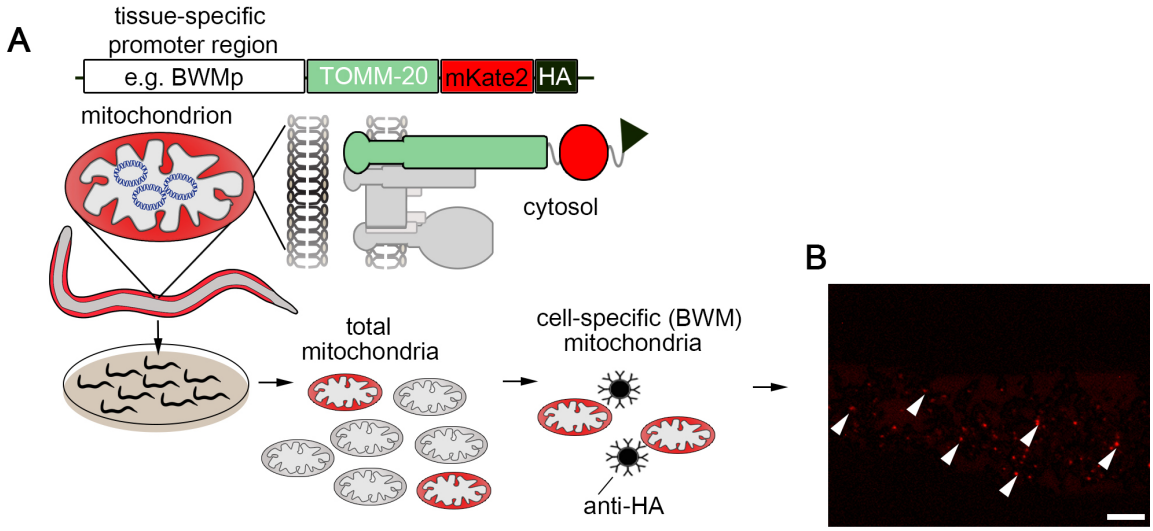

Figure S3.

(**A**) Schematic of the CS-MAP (cell-specific mitochondrial affinity purification) process to isolate mitochondria from specific tissue types in *C. elegans*. (**B**) Microscope image of purified mitochondria isolated from body wall muscle cells (white arrowheads). Scale bar, 10μm.

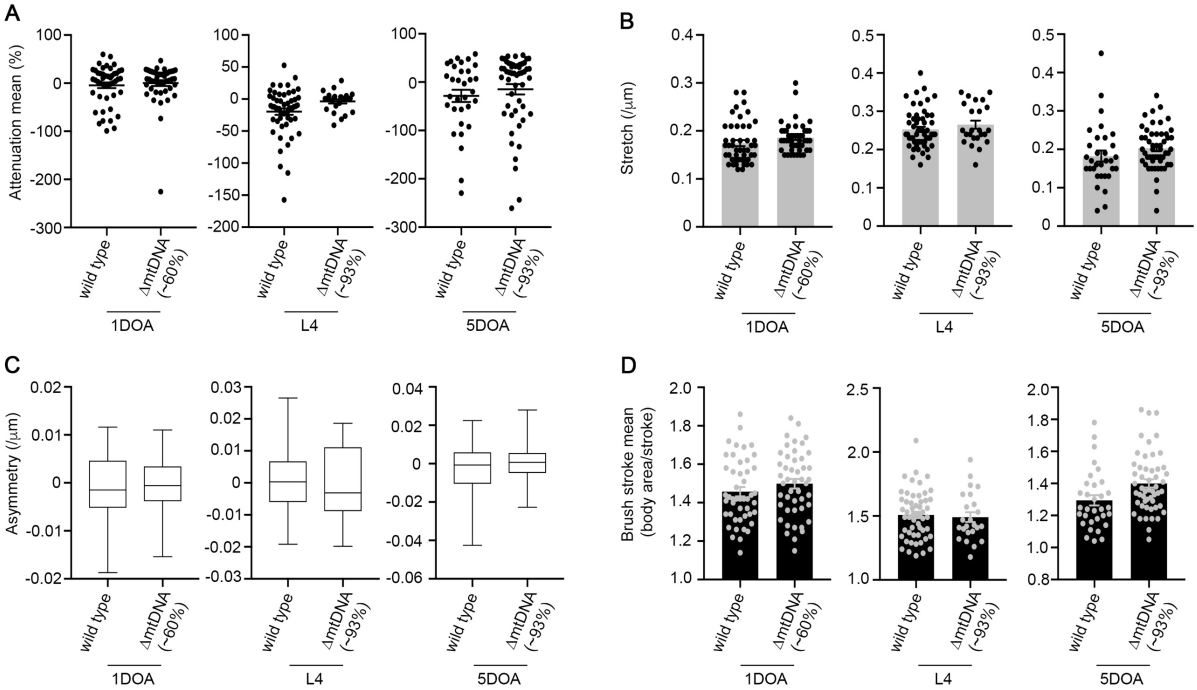

508

509

510 **Figure S4.**

511 Advanced behavioural analyses measurement show that *uaDf5* does not compromise body
512 wall muscle (BWM) function. Behavioural analyses were performed in animals harbouring the
513 *uaDf5* mtDNA mutation at different heteroplasmy levels (~60 and ~93%) and at various ages.
514 (**A**) Attenuation measures how well the depth of a body-wave is maintained as it propagates
515 from the head to the tail of the animal as it swims in liquid. It will detect any deformation in
516 BWM contraction along the length of the body. (**B**) Stretch measures the maximum
517 differences in curvature of the body. (**C**) Asymmetry evaluates how balanced the swim
518 posture is and whether the animal preferentially bends toward one side. (**D**) Brush stroke
519 evaluates the full extent of movement and flexibility of the animal. Bars and columns are
520 means ± s.e.m from individual animals (dots).

521

522

523

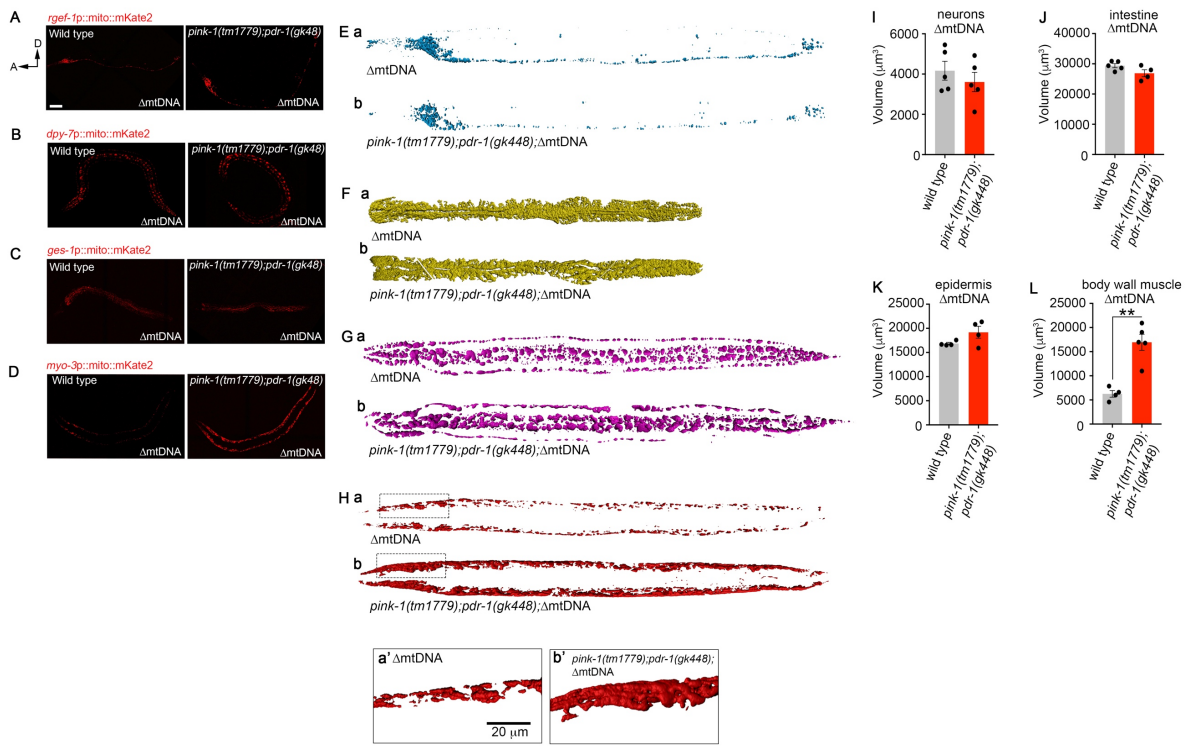

Figure S5. Deletion of *pink-1* and *pdr-1* results in an increase in mitochondrial volume in body wall muscles. (**A-D**) Representative microimages corresponding to the three-dimensional reconstructions shown in E-H. (**A**) complete nervous system mitochondria, (**B**) intestinal mitochondria, (**C**) epidermal mitochondria, and (**D**) body wall muscle mitochondria. Scale bar, 50μm. (**E-H**) Representative three-dimensional reconstructions of *C. elegans'* (**A**) complete nervous system mitochondria, (**B**) intestinal mitochondria, (**C**) epidermal mitochondria, and (**D**) body wall muscle mitochondria in (**a**) animals harbouring ΔmtDNA, and (**b**) *pink-1(tm1779);pdr-1(gk448)* animals harbouring ΔmtDNA. For (**H**), dashed boxes are magnified in (**a'-b'**). (**I-L**) Quantification of mitochondrial volumes from each tissue type. Columns are means ± s.e.m. of individual animals (n = 5). ** = p< 0.01. P values were determined using one-way ANOVA and Tukey's correction.

538 **References**

539 1. West AP, Shadel GS (2017) Mitochondrial DNA in innate immune responses and
540 inflammatory pathology. *Nat Rev Immunol* **17**: 363-375

541 2. Spinelli JB, Haigis MC (2018) The multifaceted contributions of mitochondria to
542 cellular metabolism. *Nat Cell Biol* **20**: 745-754

543 3. Gorman GS, Chinnery PF, DiMauro S, Hirano M, Koga Y, McFarland R, Suomalainen A,
544 Thorburn DR, Zeviani M, Turnbull DM (2016) Mitochondrial diseases. *Nat Rev Dis Primers* **2**:
545 16080

546 4. Morris J, Na YJ, Zhu H, Lee JH, Giang H, Ulyanova AV, Baltuch GH, Brem S, Chen HI,
547 Kung DK*, et al.* (2017) Pervasive within-Mitochondrion Single-Nucleotide Variant
548 Heteroplasmy as Revealed by Single-Mitochondrion Sequencing. *Cell Reports* **21**: 2706-2713

549 5. Hahn A, Zuryn S (2019) The Cellular Mitochondrial Genome Landscape in Disease.
550 *Trends Cell Biol* **29**: 227-240

551 6. Stewart JB, Chinnery PF (2015) The dynamics of mitochondrial DNA heteroplasmy:
552 implications for human health and disease. *Nat Rev Genet* **16**: 530-42

553 7. McManus MJ, Picard M, Chen HW, De Haas HJ, Potluri P, Leipzig J, Towheed A,
554 Angelin A, Sengupta P, Morrow RM*, et al.* (2019) Mitochondrial DNA Variation Dictates
555 Expressivity and Progression of Nuclear DNA Mutations Causing Cardiomyopathy. *Cell*
556 *Metab* **29**: 78-90 e5

557 8. Valenci I, Yonai L, Bar-Yaacov D, Mishmar D, Ben-Zvi A (2015) Parkin modulates
558 heteroplasmy of truncated mtDNA in Caenorhabditis elegans. *Mitochondrion* **20**: 64-70

559 9. Lin YF, Schulz AM, Pellegrino MW, Lu Y, Shaham S, Haynes CM (2016) Maintenance
560 and propagation of a deleterious mitochondrial genome by the mitochondrial unfolded
561 protein response. *Nature* **533**: 416-9

562 10. Gitschlag BL, Kirby CS, Samuels DC, Gangula RD, Mallal SA, Patel MR (2016)
563 Homeostatic Responses Regulate Selfish Mitochondrial Genome Dynamics in C. elegans. *Cell*
564 *Metab* **24**: 91-103

565 11. Suen DF, Narendra DP, Tanaka A, Manfredi G, Youle RJ (2010) Parkin overexpression
566 selects against a deleterious mtDNA mutation in heteroplasmic cybrid cells. *Proc Natl Acad*
567 *Sci U S A* **107**: 11835-40

568 12. Kandul NP, Zhang T, Hay BA, Guo M (2016) Selective removal of deletion-bearing
569 mitochondrial DNA in heteroplasmic Drosophila. *Nat Commun* **7**: 13100

570 13. Wang Y, Michikawa Y, Mallidis C, Bai Y, Woodhouse L, Yarasheski KE, Miller CA,
571 Askanas V, Engel WK, Bhasin S*, et al.* (2001) Muscle-specific mutations accumulate with
572 aging in critical human mtDNA control sites for replication. *Proc Natl Acad Sci U S A* **98**:
573 4022-7

574 14. Samuels DC, Li C, Li B, Song Z, Torstenson E, Boyd Clay H, Rokas A, Thornton-Wells
575 TA, Moore JH, Hughes TM*, et al.* (2013) Recurrent tissue-specific mtDNA mutations are
576 common in humans. *PLoS Genet* **9**: e1003929

577 15. Soong NW, Hinton DR, Cortopassi G, Arnheim N (1992) Mosaicism for a Specific
578 Somatic Mitochondrial-DNA Mutation in Adult Human Brain. *Nature Genetics* **2**: 318-323

579 16. Ahier A, Dai C-Y, Tweedie A, Bezawork-Geleta A, Kirmes I, Zuryn S (2018) Affinity
580 purification of cell-specific mitochondria from whole animals resolves patterns of genetic
581 mosaicism. *Nat Cell Biol* **20**: 352-360

582 17. Cortopassi GA, Shibata D, Soong NW, Arnheim N (1992) A pattern of accumulation of
583 a somatic deletion of mitochondrial DNA in aging human tissues. *Proc Natl Acad Sci U S A*
584 **89**: 7370-4

585 18. Tsang WY, Lemire BD (2002) Stable heteroplasmy but differential inheritance of a
586 large mitochondrial DNA deletion in nematodes. *Biochem Cell Biol* **80**: 645-54

587 19. Diaz F, Bayona-Bafaluy MP, Rana M, Mora M, Hao H, Moraes CT (2002) Human
588 mitochondrial DNA with large deletions repopulates organelles faster than full-length
589 genomes under relaxed copy number control. *Nucleic Acids Research* **30**: 4626-4633

590 20. Gieseler K, Qadota H, Benian GM (2017) Development, structure, and maintenance
591 of C. elegans body wall muscle. *WormBook* **2017**: 1-59

592 21. Jiang M, Kauppila TES, Motori E, Li X, Atanassov I, Folz-Donahue K, Bonekamp NA,
593 Albarran-Gutierrez S, Stewart JB, Larsson NG (2017) Increased Total mtDNA Copy Number
594 Cures Male Infertility Despite Unaltered mtDNA Mutation Load. *Cell Metab* **26**: 429-436 e4

595 22. Pickles S, Vigie P, Youle RJ (2018) Mitophagy and Quality Control Mechanisms in
596 Mitochondrial Maintenance. *Curr Biol* **28**: R170-R185

597 23. Springer W, Hoppe T, Schmidt E, Baumeister R (2005) A Caenorhabditis elegans
598 Parkin mutant with altered solubility couples alpha-synuclein aggregation to proteotoxic
599 stress. *Hum Mol Genet* **14**: 3407-23

600 24. Cummins N, Tweedie A, Zuryn S, Bertran-Gonzalez J, Götz J (2019) Disease-
601 associated tau impairs mitophagy by inhibiting Parkin translocation to mitochondria. *EMBO*
602 *J* **38**

603 25. Palikaras K, Lionaki E, Tavernarakis N (2015) Coordination of mitophagy and
604 mitochondrial biogenesis during ageing in C. elegans. *Nature* **521**: 525-8

605 26. Kirienko NV, Ausubel FM, Ruvkun G (2015) Mitophagy confers resistance to
606 siderophore-mediated killing by Pseudomonas aeruginosa. *Proc Natl Acad Sci U S A* **112**:
607 1821-6

608 27. Ryu D, Mouchiroud L, Andreux PA, Katsyuba E, Moullan N, Nicolet-Dit-Felix AA,
609 Williams EG, Jha P, Lo Sasso G, Huzard D*, et al.* (2016) Urolithin A induces mitophagy and

610 prolongs lifespan in C. elegans and increases muscle function in rodents. *Nat Med* **22**: 879-
611 88

612 28. Palikaras K, Lionaki E, Tavernarakis N (2018) Mechanisms of mitophagy in cellular
613 homeostasis, physiology and pathology. *Nat Cell Biol* **20**: 1013-1022

614 29. Harper JW, Ordureau A, Heo JM (2018) Building and decoding ubiquitin chains for
615 mitophagy. *Nat Rev Mol Cell Biol* **19**: 93-108

616 30. Samann J, Hegermann J, von Gromoff E, Eimer S, Baumeister R, Schmidt E (2009)
617 Caenorhabditits elegans LRK-1 and PINK-1 act antagonistically in stress response and neurite
618 outgrowth. *J Biol Chem* **284**: 16482-91

619 31. Polanco JC, Li C, Bodea LG, Martinez-Marmol R, Meunier FA, Götz J (2018) Amyloid-
620 beta and tau complexity - towards improved biomarkers and targeted therapies. *Nat Rev*
621 *Neurol* **14**: 22-39

622 32. Franco-Iborra S, Plaza-Zabala A, Sebastian D, Vila M, Martinez-Vicente M (2019)
623 Impairment of neuronal mitophagy by mutant huntingtin. *bioRxiv*

624 33. Gidalevitz T, Ben-Zvi A, Ho KH, Brignull HR, Morimoto RI (2006) Progressive
625 disruption of cellular protein folding in models of polyglutamine diseases. *Science* **311**:
626 1471-4

627 34. Picard M, Shirihai OS, Gentil BJ, Burelle Y (2013) Mitochondrial morphology
628 transitions and functions: implications for retrograde signaling? *Am J Physiol Regul Integr*
629 *Comp Physiol* **304**: R393-406

630 35. Trifunovic A, Wredenberg A, Falkenberg M, Spelbrink JN, Rovio AT, Bruder CE,
631 Bohlooly YM, Gidlof S, Oldfors A, Wibom R*, et al.* (2004) Premature ageing in mice
632 expressing defective mitochondrial DNA polymerase. *Nature* **429**: 417-23

633 36. Kujoth GC, Hiona A, Pugh TD, Someya S, Panzer K, Wohlgemuth SE, Hofer T, Seo AY,
634 Sullivan R, Jobling WA*, et al.* (2005) Mitochondrial DNA mutations, oxidative stress, and
635 apoptosis in mammalian aging. *Science* **309**: 481-4

636 37. Filograna R, Koolmeister C, Upadhyay M, Pajak A, Clemente P, Wibom R, Simard ML,
637 Wredenberg A, Freyer C, Stewart JB*, et al.* (2019) Modulation of mtDNA copy number
638 ameliorates the pathological consequences of a heteroplasmic mtDNA mutation in the
639 mouse. *Sci Adv* **5**: eaav9824

640 38. Ashrafi G, Schlehe JS, LaVoie MJ, Schwarz TL (2014) Mitophagy of damaged
641 mitochondria occurs locally in distal neuronal axons and requires PINK1 and Parkin. *J Cell*
642 *Biol* **206**: 655-70

643 39. Bingol B, Tea JS, Phu L, Reichelt M, Bakalarski CE, Song Q, Foreman O, Kirkpatrick DS,
644 Sheng M (2014) The mitochondrial deubiquitinase USP30 opposes parkin-mediated
645 mitophagy. *Nature* **510**: 370-5

646 40. Pickrell AM, Huang CH, Kennedy SR, Ordureau A, Sideris DP, Hoekstra JG, Harper JW,
647 Youle RJ (2015) Endogenous Parkin Preserves Dopaminergic Substantia Nigral Neurons
648 following Mitochondrial DNA Mutagenic Stress. *Neuron* **87**: 371-81

649 41. Valente EM, Abou-Sleiman PM, Caputo V, Muqit MM, Harvey K, Gispert S, Ali Z, Del
650 Turco D, Bentivoglio AR, Healy DG*, et al.* (2004) Hereditary early-onset Parkinson's disease
651 caused by mutations in PINK1. *Science* **304**: 1158-60

652 42. Kitada T, Asakawa S, Hattori N, Matsumine H, Yamamura Y, Minoshima S, Yokochi M,
653 Mizuno Y, Shimizu N (1998) Mutations in the parkin gene cause autosomal recessive juvenile
654 parkinsonism. *Nature* **392**: 605-8

655 43. Kraytsberg Y, Kudryavtseva E, McKee AC, Geula C, Kowall NW, Khrapko K (2006)
656 Mitochondrial DNA deletions are abundant and cause functional impairment in aged human
657 substantia nigra neurons. *Nat Genet* **38**: 518-20

658 44. Bender A, Krishnan KJ, Morris CM, Taylor GA, Reeve AK, Perry RH, Jaros E, Hersheson
659 JS, Betts J, Klopstock T*, et al.* (2006) High levels of mitochondrial DNA deletions in substantia
660 nigra neurons in aging and Parkinson disease. *Nat Genet* **38**: 515-7

661 45. Brenner S (1974) The genetics of Caenorhabditis elegans. *Genetics* **77**: 71-94

662 46. Restif C, Ibanez-Ventoso C, Vora MM, Guo SZ, Metaxas D, Driscoll M (2014) CeleST:
663 Computer vision software for quantitative analysis of C. elegans swim behavior reveals
664 novel features of locomotion. *Plos Comp Biol* **10**
665